



$\text{Li}_{1.1}\text{Na}_{0.1}\text{Mn}_{0.534}\text{Ni}_{0.133}\text{Co}_{0.133}\text{O}_2$ as cathode with ameliorated electrochemical performance based on dual Li^+/Na^+ electrolyte

Yu Zhou^{1,2} · Xianhua Hou^{1,2} · Kaixiang Shen^{1,2} · Shaofeng Wang^{1,2} · Fuming Chen^{1,2} · Yajie Li^{1,2} · Hedong Chen^{1,2} · Bei Wang^{1,2}

Received: 8 March 2018 / Revised: 11 April 2018 / Accepted: 3 May 2018 / Published online: 11 May 2018
© Springer-Verlag GmbH Germany, part of Springer Nature 2018

Abstract

Layered Li-rich cathode materials $\text{Li}_{1.2}\text{Mn}_{0.534}\text{Ni}_{0.133}\text{Co}_{0.133}\text{O}_2$ (LNCMN-0) and Na doping $\text{Li}_{1.1}\text{Na}_{0.1}\text{Mn}_{0.534}\text{Ni}_{0.133}\text{Co}_{0.133}\text{O}_2$ (LNCMN-0.1) are prepared successfully by a co-precipitation method and several consecutive calcination treatments. Besides, the phase structure, morphology, and electrochemical properties of the four samples are studied in detail using X-ray diffraction (XRD), scanning electron microscope (SEM), galvanostatic charge-discharge test, cyclic voltammetry (CV), and electrochemical impedance spectroscopy (EIS). Although the discharge capacity of spherical LNCMN-0.1 decreases slightly at 0.1 C (1 C = 250 mA g⁻¹), compared to the pristine LNCMN-0, it is noteworthy that the LNCMN-0.1 matched with dual Li^+/Na^+ electrolyte exhibit superior stability performance at 1 C, as well as enhanced rate capability. The LNCMN-0.1 (Li^+/Na^+) delivers an initial discharge specific capacity of 267.61 mAh g⁻¹ at 0.1 C between 2.0 and 4.8 V at room temperature and initial coulombic efficiency of 83.51%, which is higher than the LNCMN-0 samples (76.42 and 81.54%). The experimental results verify that Na doping combined with dual Li^+/Na^+ electrolyte can generate a synergistic effect, which is a promising idea to ameliorate the electrochemical performance for this material.

Keywords Li-rich layered cathode materials · Na doping · Dual Li^+/Na^+ electrolyte · Synergistic effect

Introduction

Nowadays, with global shortage of oil resources, many efforts have been adopted to promote the development of new energy vehicles industry. Lithium-ion batteries (LIBs) have been brought into focus by virtue of its advantages of high energy density, high storage capacity, and long cycling life.[1–5] Hence, LIBs have been applied in many electronic devices including mobile phones, laptop computers, and hybrid electric vehicles and pure electric taxis or busses [6–8].

It is well known that cathode materials play a significant role in application of LIBs. Lithium cobalt oxide (LiCoO_2) [9] is the earliest to be researched and widely used commercial cathode material for LIBs, resulting from its facile synthesis route, low self-discharge, excellent cycle lifespan, and high energy density. However, its major defects are costly cobalt, [10] fast capacity decline at higher rates [11], and its rapid capacity loss above 4.4 V (vs. Li^+/Li).[12] With years of investigation and exploration, numerous alternative cathode materials with cost-effective and ameliorated performance have been studied to improve the drawbacks of LiCoO_2 , including LiFePO_4 [13, 14], LiMn_2O_4 [15, 16], Li-O [17], Li-S [18], $\text{LiNi}_x\text{Mn}_{2-x}\text{O}_4$ [19], $\text{LiNi}_x\text{Co}_y\text{Mn}_{1-x-y}\text{O}_2$ (NCM) [20], and $\text{Li}_{1.2}\text{Ni}_x\text{Co}_y\text{Mn}_2\text{O}_2$ [6]. Notably, layered lithium nickel-cobalt-manganese oxides not only integrate individual advantages of LiNiO_2 , LiCoO_2 , and LiMnO_2 , but also reduce the content of costly and toxic cobalt [21–23]. Therefore, the composite system of $\text{LiNi}_x\text{Co}_y\text{Mn}_{1-x-y}\text{O}_2$ (NCM) has become an area of research focus. But the NCM still suffers from some drawbacks of capacity fade, voltage decay [13], and poor rate capability, which restrict their further applications.

✉ Xianhua Hou
houxianhua@m.scnu.edu.cn

¹ Guangdong Provincial Key Laboratory of Quantum Engineering and Quantum Materials, School of Physics and Telecommunication Engineering, South China Normal University, Guangzhou 510006, People's Republic of China

² Guangdong Engineering Technology Research Center of Efficient Green Energy and Environment Protection Materials, Guangzhou 510006, People's Republic of China

In many released reports, coating and doping have been detected as efficient strategies to conquer these drawbacks above. Surface coating modification, which can form a protective layer around electrode materials, is capable to alleviate erosion of hydrofluoric acid decomposed from electrolyte in the charge-discharge processes. Lu et al. [24] studied that CeF₃-coated lithium-rich layered Li_{1.2}Mn_{0.54}Ni_{0.13}Co_{0.13}O₂ exhibits better cyclic performance and capacity retention.

In addition to surface coating, there are some researches regard to a certain amount of element doping. Wang et al. [25] researched LiMnPO₄ by boron doping at P-site improved electrochemical performance. Xie et al. [26] reported the sodium-doped LiNi_{0.8}Co_{0.15}Al_{0.05}O₂ displays improved capacity retention and satisfactory performance at high rates, similarly, defined as pillar effect [13]. Guo et al. [14] investigated that Na additive samples demonstrate large reversible capacity, prolonged cycling stability in comparison with the bare sample. The abovementioned literatures effectively enhance the transfer dynamics of ions and electrons for the positive electrode materials and further improve the cycling stability.

In order to improve the electrochemical performance of layered Li-rich Li_{1.2}Mn_{0.534}Ni_{0.133}Co_{0.133}O₂, we take Na doping into consideration in this work. Apparently, after Na doping into cathode materials, the electrode contains Li and Na element, whereas the most common electrolyte of LIBs that is LiPF₆ dissolved in ethylene carbonate (EC) and dimethyl carbonate (DMC), merely involves Li⁺ and no Na⁺. Moreover, in charge process cathode materials will lose electrons, and then forming Li⁺ and Na⁺ on the surface of electrode materials. Afterwards, Li⁺ transported through LiPF₆ electrolyte produces intercalation and de-intercalation back and forth between the two electrodes in the cycling processes; nevertheless, Na⁺ cannot be conveyed to reference electrode, namely no sufficient exhibition relative to the function of dual Li⁺/Na⁺. Thereby, the impact on performance of mixed electrolyte needs to be further explored. In particular, element doping combined with mixed electrolyte, if generating a synergistic effect, would be a meaningful amelioration method. In this article, we have not only synthesized Li_{1.1}Na_{0.1}Mn_{0.534}Ni_{0.133}Co_{0.133}O₂ (LNCMN-0.1) hybrids acting as cathode materials via a facile coprecipitation method [24, 27] and reported a novel idea to fabricate LNCMN-0.1 using dual Li⁺/Na⁺ electrolyte, but also investigated the effects of Na additive on phase structure, morphology, and electrochemical properties. Experimental results suggest that the LNCMN-0.1 (Li⁺/Na⁺), indeed, form a synergistic effect, namely, achieving mutual diffusion of Li⁺ and Na⁺ and accordingly increasing the ionic mobility and electronic conductivity during cycling processes.

Experimental section

Synthesis of spherical Li-rich materials

In typical, Mn(CH₃COO)₂·4H₂O, Ni(CH₃COO)₂·4H₂O, and Co(CH₃COO)₂·4H₂O whose molar ratio is Mn:Ni:Co of 0.534:0.133:0.133 (1.0 M) were dissolved together in 100 mL distilled water to obtain a transparent solution. Then, a mixed solution containing 120 mL of Na₂CO₃ (1.0 M) and the transition metal acetate solution was gradually added to 300 mL of NH₄HCO₃ (0.5 M). The pH was adjusted to 8–9 using NH₄OH followed by vigorously stirring for 5 h with a stirring speed of 800 rpm. The obtained precipitates were then filtrated, rinsed with distilled water, and finally dried at 60 °C for 8 h. The dried powder of metal carbonate precursor was mixed with Li₂CO₃ (5 wt% excess) and Na₂CO₃ (molar ratio of Li:Na = 1.1:0.1) and then grind to make of even mixture. Finally, the mixture was preheated at 500 °C for 5 h, 720 °C for 5 h and calcined at 900 °C for 12 h in air atmosphere to obtain the target compound of Li_{1.1}Na_{0.1}Mn_{0.534}Ni_{0.133}Co_{0.133}O₂ (LNCMN-0.1). The LNCMN-0.1 assembled with dual Li⁺/Na⁺ electrolyte and merely Li⁺ electrolyte, are named as LNCMN-0.1 (Li⁺/Na⁺) and LNCMN-0.1 (Li⁺), respectively.

For comparison, Li_{1.2}Mn_{0.534}Ni_{0.133}Co_{0.133}O₂ (the LNCMN-0) has also been prepared using the same method, only without adding Na₂CO₃ in grinding process. The LNCMN-0 assembled with dual Li⁺/Na⁺ electrolyte and simply Li⁺ electrolyte, are named as LNCMN-0 (Li⁺/Na⁺) and LNCMN-0 (Li⁺), respectively.

Material characterization and electrochemical measurements

X-ray diffraction (XRD, PANalytical X' Pert PRO, Cu-Kα radiation, λ = 0.15406 Å) was utilized to characterize the phase structure of the as-prepared samples. The XRD patterns were obtained in a 2θ range from 10 to 80° at a scan rate of 0.02° s⁻¹. The morphologies of samples were characterized by scanning electron microscopy (SEM, ZEISS ULTRA 55).

Electrochemical measurements were performed in coin-type half-cells (CR2430) assembled in an argon-filled glove box. The working electrode was fabricated with 80 wt% LNCMN-0.1 or LNCMN-0 as active materials, 10 wt% acetylene black (conductive agent), and 10 wt% PVDF (the binder). The obtained slurry was printed on aluminum foil (approximate 10 μm thickness) and then dried under vacuum at 60 °C for 12 h. Afterwards, the electrodes were roll-pressed and punched (φ = 18 mm). The coating mass on the Al foil was 6.0 mg averagely. Lithium foil was used as the reference electrode and Celgard-2400 as the separator. The dual Li⁺/Na⁺ electrolyte was 1 M LiPF₆:1 M NaPF₆ = 1.1:0.1 (v:v) dissolved in EC:DMC = 1:1 (v:v). The charge-discharge tests

was conducted by NEWARE Battery Testing System in the voltage range of 2.0 to 4.8 V (vs. Li/Li⁺) at a constant current densities from 0.1 to 10 C (1 C = 250 mA g⁻¹) at room temperature. Cyclic voltammograms (CV) were carried out on a Solartron Analytical 1470E electrochemical workstation at different sweep speeds of 0.05, 0.1, 0.2, and 0.5 mV s⁻¹ between 2.0 and 4.65 V. And the electrochemical impedance spectroscopy (EIS) was conducted using CHI604D Electrochemistry System at an open voltage in the frequency range from 100 kHz to 0.01 Hz with a voltage amplitude of 10 mV.

Results and discussion

As illustrated in Scheme 1, the spherical Li_{1.1}Na_{0.1}Mn_{0.534}Ni_{0.133}Co_{0.133}O₂ is prepared successfully by a facile co-precipitation method with several consecutive calcination treatments. It shows that the smooth surface of the precursor apparently changes to a layer-by-layer morphology.

The XRD patterns of the LNCMN-0.1 and the LNCMN-0 are shown in Fig. 1. The main peaks (around 2θ = 18.6, 37.0, and 44.7°) are clearly observed in both samples, which can be indexed to the layered hexagonal α-NaFeO₂ structure with a space group of R-3m [24]. There is no other diffraction peaks, indicating that the alien atoms do not destroy the lattice structure of LNCMN-0 and no impurity phase. In addition, the clear splitting peaks of (006)/(012) and (018)/(110) also indicate ordered layered structure [7]. Furthermore, the XRD patterns and the insert graph illustrate that the peaks of Na doping sample present slightly shift towards to left in the 2θ range of 36–46°, indicating an influence of enlarging the lattice volume due to the pillar effects [13] of Na doping. With larger radius of Na⁺ (0.102 nm) than Li⁺ (0.076 nm), the alien Na can enlarge Li layers spacing and crystal size and provide larger space for the movement of ions and electrons. The weak lattice peaks at 20 to 25° are indexed to the monoclinic Li₂MnO₃-like domains with space group of C2/m [6]. The Na doping sample can restrain layered-to-spinel phase transition [26], which may ascribe to improve structural stability and reduce the cation mixing by the addition of Na [28, 29].

The morphology of the precursor, pristine LNCMN-0, and LNCMN-0.1 is shown in Fig. 2. All the samples are comprised of spherical particles with a particle diameter of 1–6 μm. In Fig. 2a and b, the precursor particle displays low degree of crystallinity. Meanwhile, there is no apparent morphology transformation observed for both cathode material particles, which manifests that Na doping may not influence the morphology of pristine LNCMN-0 particles. However, some small flakes and voids exist on the surface of the LNCMN-0.1 particles. The tiny flakes may form as an amorphous phase during the high temperature annealing of crystal growth because there is no evident crystallization phase for any impure components shown in the XRD patterns [26]. In addition, the voids occur accordingly when the primary particles aggregate together and form spherical secondary particles.

Figure 3 illustrates the transportation of Li⁺ and Na⁺ during the discharge process. Firstly, Li⁺ and Na⁺ are transported by individual carrier (LiPF₆ and NaPF₆) through the separator and interface film between electrode and electrolyte into the surface of cathode (Li_{1.1}Na_{0.1}M_{0.8}O₂, M = Ni, Co, Mn). The electron moves from the external circuit into the cathode. Afterwards, Li⁺, Na⁺, and transition metal ions obtain several electrons and generate a series of reduction reactions.

The cycling performances for four samples are measured at 1 C for 55 cycles after 0.1 C for 3 cycles at the voltage range of 2.0–4.8 V. As delivered in Fig. 4a, despite a slight decrease of specific capacity at 0.1 C for Na doping samples, the LNCMN-0.1 (Li⁺/Na⁺) and LNCMN-0.1 (Li⁺) exhibit superior cycle stability than the other two pristine samples. Among the four samples, the LNCMN-0.1 (Li⁺/Na⁺) presents the excellent discharge specific capacity of 172.04 mAh g⁻¹ and capacity retention of 85.79% at 1 C after 50 cycles, while the LNCMN-0 (Li⁺/Na⁺) shows inferior discharge specific capacity of 138.09 mAh g⁻¹ and capacity retention of 73.91% in the same test conditions. The initial coulombic efficiency of LNCMN-0.1 (Li⁺/Na⁺), LNCMN-0.1 (Li⁺), LNCMN-0 (Li⁺/Na⁺), and LNCMN-0 (Li⁺) are 83.51, 81.76, 76.42, and 81.54%, respectively. Further, the initial charge-discharge profiles of LNCMN-0 (Li⁺/Na⁺) and LNCMN-0.1 (Li⁺/Na⁺) are presented in Fig. 4b. Both cathode materials exhibit two plateaus at 4.0–4.4 V and above 4.5 V during the initial charge

Scheme 1 Illustration of co-precipitation followed with subsequent calcinations for the formation of LNCMN-0.1

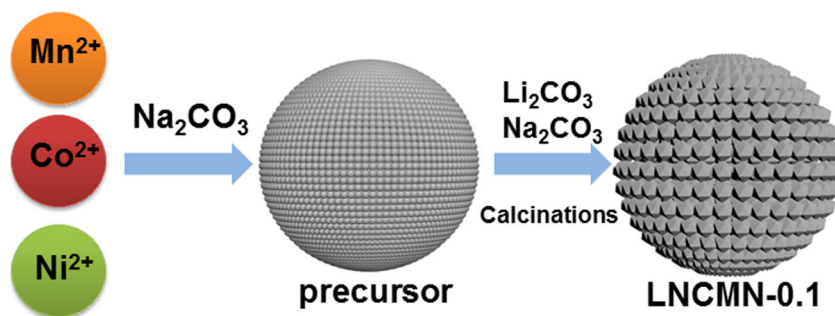
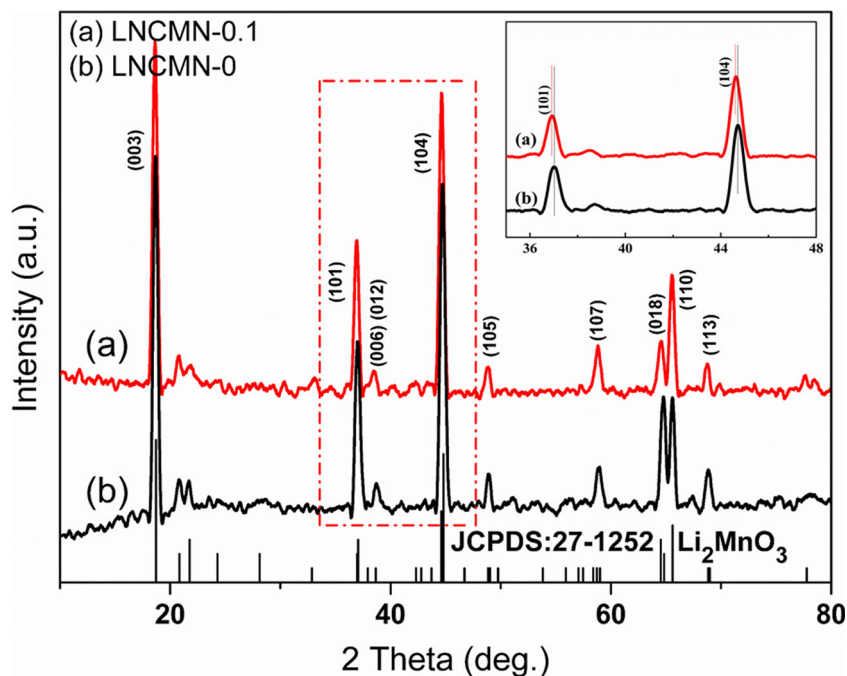


Fig. 1 The XRD patterns of **a** the LNCMN-0.1 and **b** the LNCMN-0



process, which is corresponding to two different Li^+ deintercalation and polarization processes [6]. Apparently, it also shows that the initial coulombic efficiency and initial charge/discharge specific capacity of the LNCMN-0.1 (Li^+/Na^+) electrode is 83.51% and 320.42/267.61 mAh g^{-1} at 0.1 C, higher than that of the LNCMN-0 (Li^+/Na^+), which is 76.42% and 351.32/268.49 mAh g^{-1} .

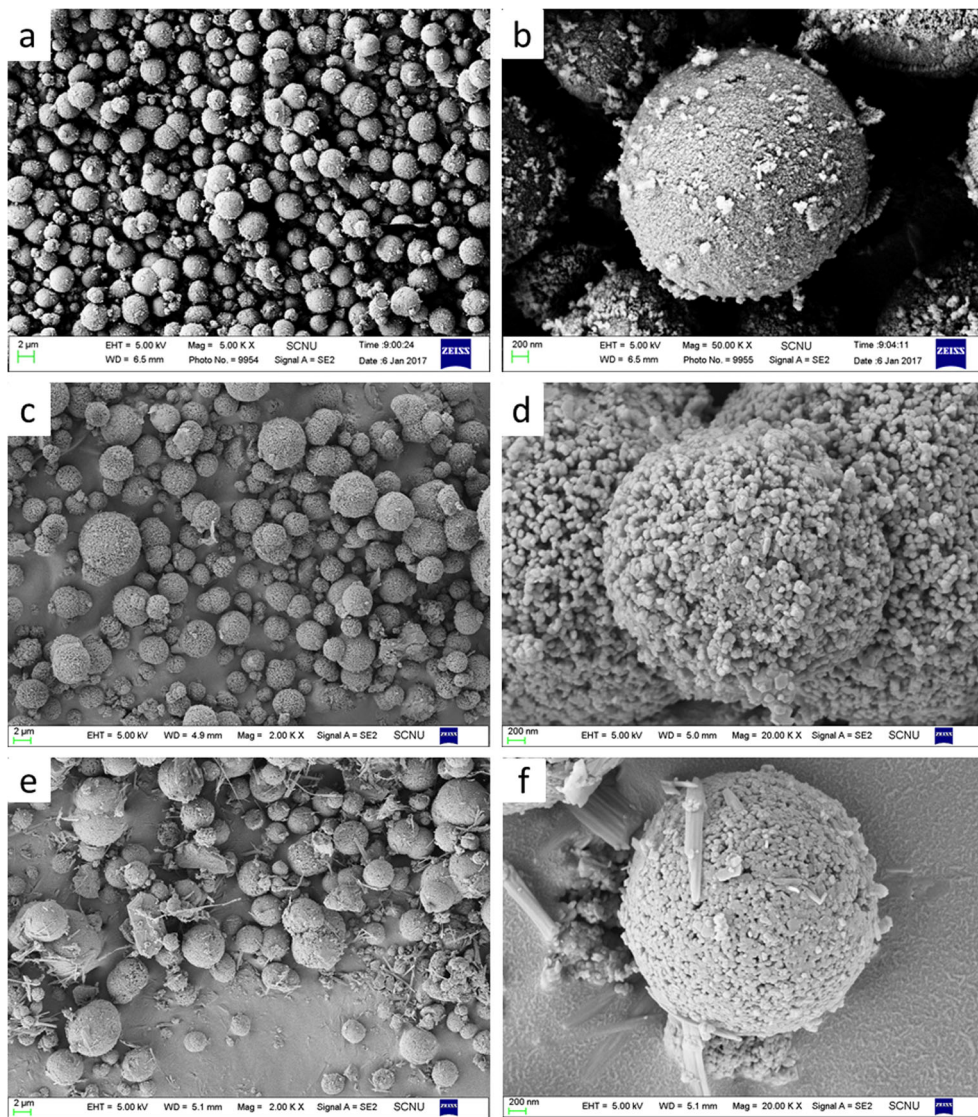
Moreover, Fig. 4c delivers the rate capability of LNCMN-0.1 (Li^+/Na^+), LNCMN-0.1 (Li^+) and LNCMN-0 (Li^+/Na^+) under galvanostatic charge and discharge test at different rates from 0.1 to 10 C. Although the LNCMN-0.1 (Li^+/Na^+) and LNCMN-0.1 (Li^+) show a bit low reversible capacity at 0.1 C, compared to the LNCMN-0 (Li^+/Na^+), they exhibit higher discharge capacity at higher rates from 0.5 to 10 C. Such superior rate capability of LNCMN-0.1 (Li^+/Na^+) and LNCMN-0.1 (Li^+) might be ascribed to Na doping enlarging layer spacing [26] that is conducive to accelerate ion transportation and electron conductivity and well exert synergistic effect between Na doping and dual Li^+/Na^+ electrolyte. More remarkable, when the current density returns back to 0.1 C, the discharge capacity of the Na doping samples can almost revert to its initial capacity, while the LNCMN-0 (Li^+/Na^+) recovers to merely 76.85% of that. The results reveal that the LNCMN-0.1 may mitigate the influence at high current density and possess preferable structural stability at diverse rates. Moreover, Na doping combined dual Li^+/Na^+ electrolyte indeed create favorable effect, which verifies in our original assumption—synergistic effect.

In order to detect the redox reactions on the surface of electrode and electrolyte during cycling, cyclic voltammetry (CV) measurements are performed [2]. As shown in Fig. 5a, b,

CV profiles of the first 3 cycles are presented at a scan rate of 0.1 mV s^{-1} between 2.0 and 4.65 V. Obviously, it can be observed that the plots of LNCMN-0.1 (Li^+/Na^+) are overlapped well than that of the LNCMN-0 (Li^+), indicating that the former will exhibit better reversibility of the electrode reactions, which is accord with the stable cycling results in Fig. 4a. The CV curves of LNCMN-0 (Li^+) and LNCMN-0.1 (Li^+/Na^+) both exhibit two oxidation peaks in the anodic scan, which could be attributed to the delithiation. The first peak at ~ 4.1 V is related to the oxidation of Ni^{2+} to Ni^{4+} and Co^{3+} to Co^{4+} , while the second peak at ~ 4.6 V merely refers to the oxidation of Co^{3+} to Co^{4+} [6]. The corresponding voltage values of the peaks are consistent with the plateaus in initial charge-discharge plots in Fig. 4b. Moreover, Mn^{4+} in the electrode as a structural material does not take part in a chemical reaction during the charge and discharge cycles, which can keep the structural stability of LNCMN-0 and LNCMN-0.1. In the reversal cathodic sweep, the reduction peaks at ~ 3.3 and ~ 3.82 V are attributed to the reduction of Ni^{4+} to Ni^{2+} and Co^{4+} to Co^{3+} [30]. In addition, the LNCMN-0.1 (Li^+/Na^+) has a smaller difference for redox peak potential ($\Delta V = 0.24$ V) than the LNCMN-0 (Li^+) ($\Delta V = 0.38$ V), which may ascribe to slightly suppress polarization process and irreversible side reaction [31, 32].

Figure 5c, d exhibits the CV profiles of the LNCMN-0 (Li^+) and LNCMN-0.1 (Li^+/Na^+) at different scan speeds (0.05, 0.1, 0.2, and 0.5 mV s^{-1}) at 2.0–4.65 V. The figures display that the peak intensity increases with the increase of sweep speed for both samples. Besides, Fig. 5e, f show the fitting plots of oxidation and reduction peak currents ($10^3 i_p$)

Fig. 2 The SEM images of **a, b** the precursor; **c, d** the LNCMN-0; and **e, f** the LNCMN-0.1



vs. the square root of sweep speed. The diffusion coefficient of Li^+ can be calculated using the following equation [33]:

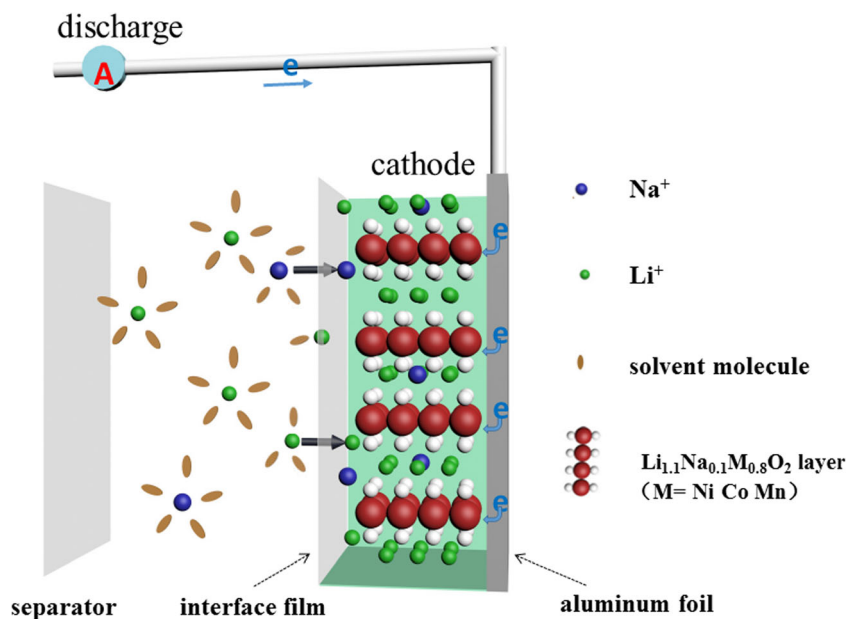
$$i_p = (2.69 \times 10^5) n^{3/2} A D_{\text{Li}^+}^{1/2} C v^{1/2}$$

where n denotes the number of electrons per molecule during oxidation (here, $n = 1$), A signifies the surface area of electrode (2.54 cm^2), D_{Li^+} indicates the Li^+ diffusion coefficient, C is the concentration of Li^+ ($C_{\text{LNCMN-0}} = 6.10 \times 10^{-2} \text{ mol cm}^{-3}$, $C_{\text{LNCMN-0.1}} = 5.59 \times 10^{-2} \text{ mol cm}^{-3}$), and v is the sweep speed. The D_{Li^+} of the LNCMN-0.1 (Li^+/Na^+) for oxidation and reduction peaks are 1.09×10^{-11} and $3.01 \times 10^{-12} \text{ cm}^2 \text{ s}^{-1}$, respectively, while those of the LNCMN-0 (Li^+) are 7.28×10^{-13} and $1.65 \times 10^{-13} \text{ cm}^2 \text{ s}^{-1}$, accordingly. The LNCMN-0.1 (Li^+/Na^+) sample manifests a boosted Li^+ diffusion coefficient, which may owing to the mixed Li^+/Na^+ electrolyte that is beneficial to improve the mutual

ions diffusion rate. The calculated diffusion coefficients of Li^+ also reflect well with the variation tendency of rate capability in Fig. 4c.

To further understand the effect of Na doping and dual Li^+/Na^+ electrolyte on the electrode resistance, electrochemical impedance spectroscopy (EIS) analysis [34, 35] is carried out in the fully discharge state. The measurements are imposed at 0.1 C with voltage range from 2.0 to 4.8 V before cycle and fifth cycle, respectively. As illustrated in Fig. 6, the Nyquist plots for three electrodes are all composed of a depressed semicircle in the high to medium frequency region and a slope line in the low frequency region [24]. R_s is related to the solution resistance resulting from decomposition of electrolyte when electrode is cycling in the high voltage. The semicircle signifies the charge transfer resistance (R_{ct}) in the electrode/electrolyte interface. The slope represents the Warburg impedance (W_O) which denotes the diffusion impedance of Li^+ in the bulk. In addition, CPE (constant

Fig. 3 The illustration model of Li^+ and Na^+ transportation



phase element) corresponds to the non-ideal double-layer capacitance. To estimate the value of R_s and R_{ct} , the

equivalent circuit model is used to fit the experimental results in the inset of Fig. 6.

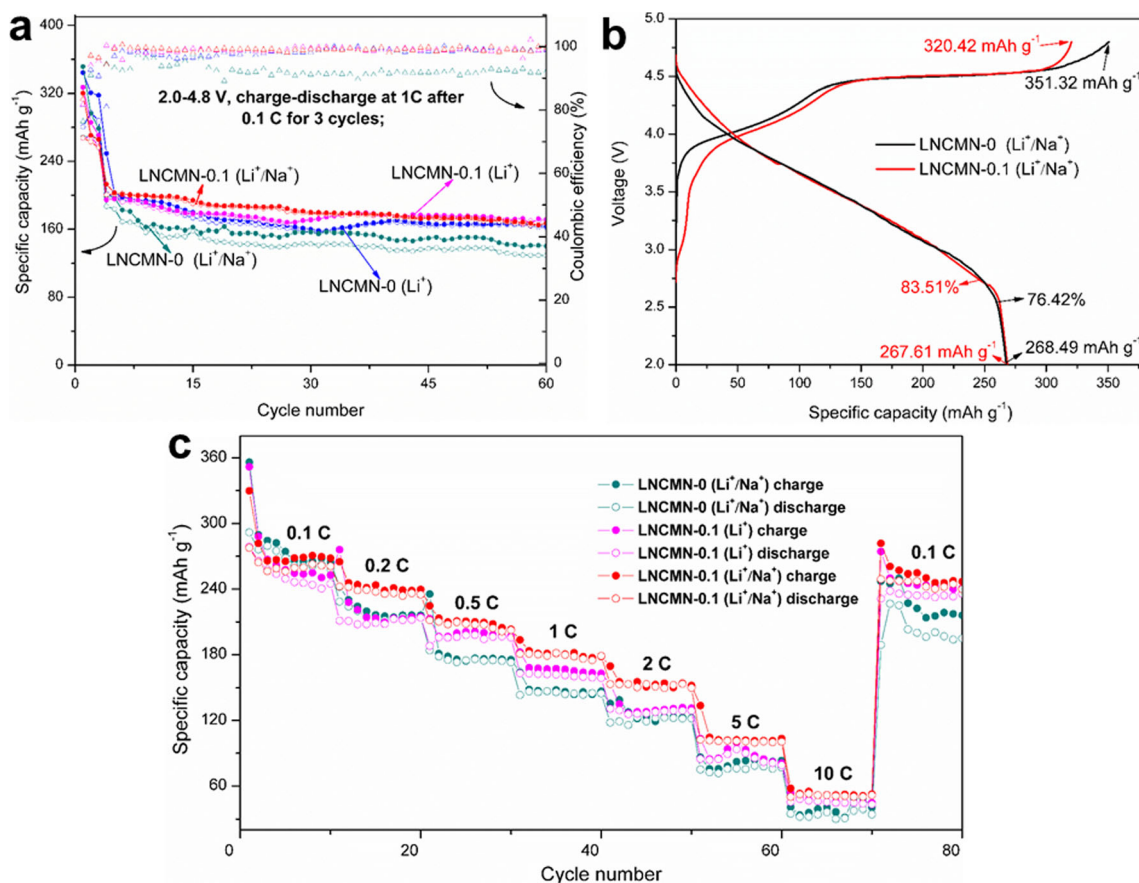
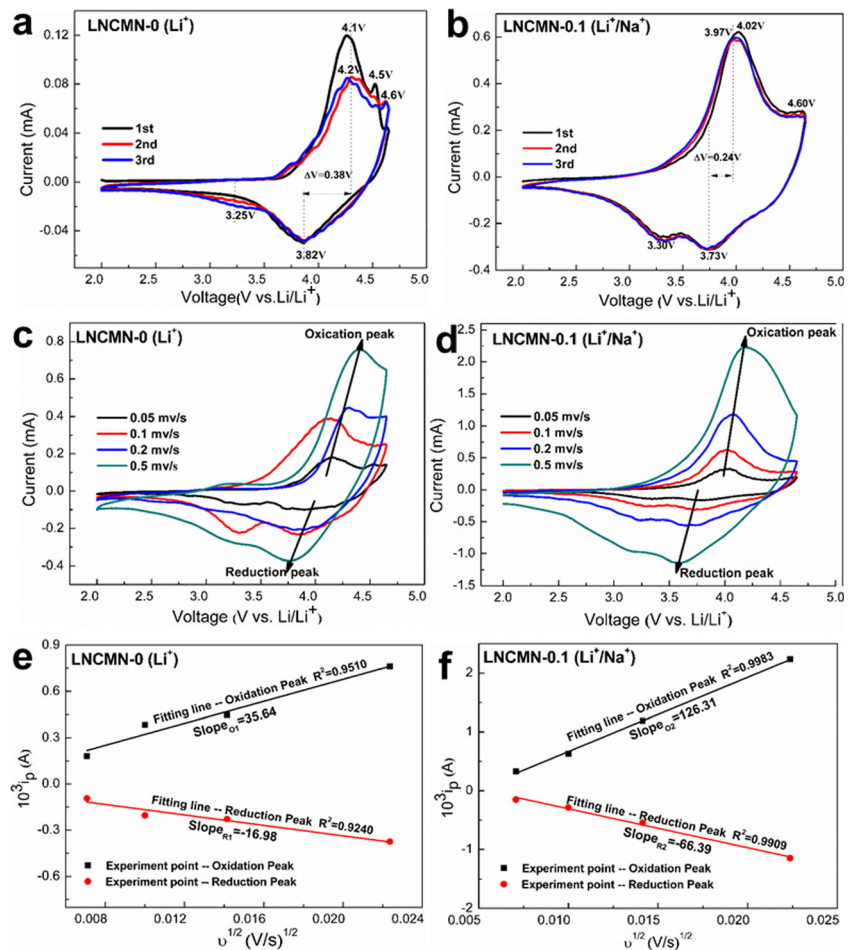


Fig. 4 **a** Cycling performance of LNCMN-0.1 (Li^+/Na^+), LNCMN-0.1 (Li^+), LNCMN-0 (Li^+/Na^+) and LNCMN-0 (Li^+) at 1 C after 0.1 C for 3 cycles. **b** Initial charge-discharge profiles at 0.1 C for LNCMN-0 (Li^+ /

Na^+) and LNCMN-0.1 (Li^+/Na^+). **c** Rate performances of LNCMN-0.1 (Li^+/Na^+), LNCMN-0.1 (Li^+) and LNCMN-0 (Li^+/Na^+)

Fig. 5. CV measured for the first 3 cycles of **a** the LNCMN-0 (Li⁺) and **b** the LNCMN-0.1 (Li⁺/Na⁺). CV measured at different sweep speeds of 0.05, 0.1, 0.2, and 0.5 mV s⁻¹ for **c** the LNCMN-0 (Li⁺) and **d** the LNCMN-0.1 (Li⁺/Na⁺). The current of peaks (10³*i*_p) vs. the square root of scanning speeds (*v*^{1/2}) plots of **e** the LNCMN-0 (Li⁺) and **f** the LNCMN-0.1 (Li⁺/Na⁺)



As listed in Table 1, there are no noticeable changes for R_s values of three electrodes after 5 cycles. It indicates the slow decomposition of electrolyte during cycling. Distinctively, the

R_{ct} values of them manifest over doubled changes with cycles. Among them, the LNCMN-0 (Li⁺/Na⁺) and LNCMN-0.1 (Li⁺/Na⁺) show the maximum (111.20 Ω) and the minimum

Fig. 6 EIS curves of LNCMN-0 (Li⁺/Na⁺), LNCMN-0.1 (Li⁺), and LNCMN-0.1 (Li⁺/Na⁺) and equivalent circuit in the inset

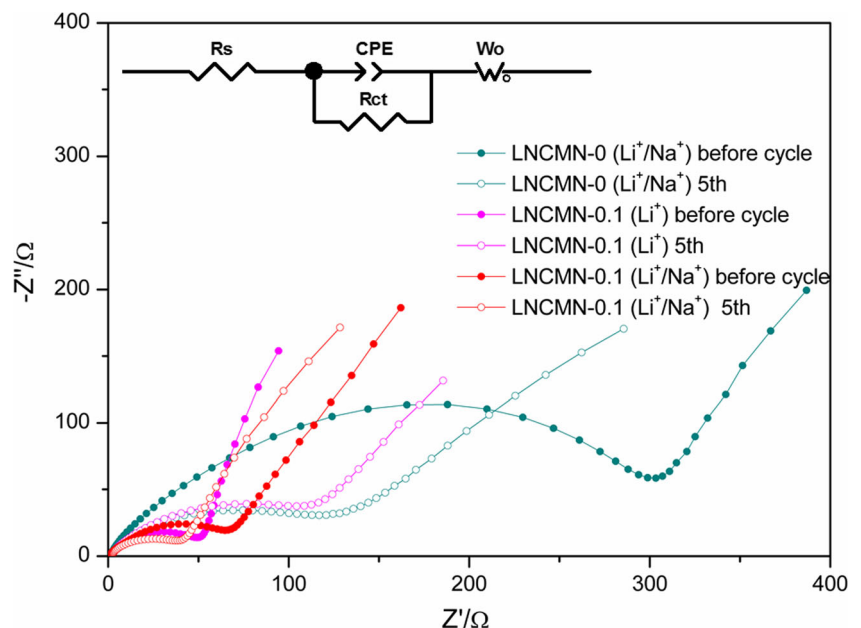


Table 1 The values of R_s and R_{ct} for the LNCMN-0 (Li^+/Na^+), LNCMN-0.1 (Li^+), and the LNCMN-0.1 (Li^+/Na^+) electrodes before cycle and after 5 cycles

Samples	R_s		R_{ct}	
	Before cycle	5th	Before cycle	5th
LNCMN-0 (Li^+/Na^+)	1.05 Ω	0.65 Ω	321.00 Ω	111.20 Ω
LNCMN-0.1 (Li^+)	1.14 Ω	1.23 Ω	51.79 Ω	108.50 Ω
LNCMN-0.1 (Li^+/Na^+)	0.73 Ω	1.55 Ω	70.76 Ω	38.58 Ω

resistance value (38.58 Ω) after 5 cycles, respectively. And the LNCMN-0.1 (Li^+) shows the R_{ct} value of 51.79 Ω before cycle and 108.50 Ω after 5 cycles, while the LNCMN-0.1 (Li^+/Na^+) shows lower R_{ct} value of 70.76 and 38.58 Ω , accordingly. From the above results, the original R_{ct} values of them are closer. The R_{ct} value for LNCMN-0.1 using LiPF_6 increases more than twice from 51.79 to 108.50 Ω after 5 cycles. On the contrary, the R_{ct} value of the LNCMN-0.1 using dual Li^+/Na^+ electrolyte decreases almost half from 70.76 to 38.58 Ω after cycling.

The marked difference of R_{ct} reveals that Na doping electrode could effectively suppress electrochemical polarization. Moreover, by the comparison of the LNCMN-0.1 (Li^+) and LNCMN-0.1 (Li^+/Na^+) electrodes, the decreased R_{ct} value suggests that electrode fabricated with dual Li^+/Na^+ electrolyte is more conducive to reducing impedance [36] and accordingly increasing ion diffusion rate during the cycling processes when compared to merely Li^+ electrolyte. On the basis of the above analysis, we can conclude that the EIS results reflect well on the ameliorated rate capability as shown in Fig. 4.

Conclusions

In conclusion, the Li-rich layered $\text{Li}_{1.1}\text{Na}_{0.1}\text{Mn}_{0.534}\text{Ni}_{0.133}\text{Co}_{0.133}\text{O}_2$ (LNCMN-0.1) electrode material was obtained successfully by a co-precipitation method and several consecutive calcination treatments. By doping a small amount of Na and adopting dual Li^+/Na^+ electrolyte in assembling process, the LNCMN-0.1 (Li^+/Na^+) cathode material exhibited good cycling stability and rate capacity at high current density. Despite a slightly reduction of initial discharge capacity at 0.1 C, initial coulombic efficiency of the LNCMN-0.1 (Li^+/Na^+) is 83.51%, higher than LNCMN-0 (Li^+/Na^+). The LNCMN-0.1 (Li^+/Na^+) can achieve a synergistic effect of Na doping combined with dual Li^+/Na^+ electrolyte, which is conducive to enhancing performance at high rates, suppressing

polarization process in the interface between electrode and electrolyte and declining the electrochemical impedance, namely accelerating ionic mobility and electronic conductivity. In consequence, this work demonstrates a promising idea to ameliorate electrochemical performance for Li-rich layered $\text{Li}_{1.2}\text{Mn}_{0.534}\text{Ni}_{0.133}\text{Co}_{0.133}\text{O}_2$ cathode materials.

Funding information This work is financially supported by the union project of National Natural Science Foundation of China and Guangdong Province (No. U1601214), the Scientific and Technological Plan of Guangdong Province (2016B010114002, 2017B090901027), the Scientific and Technological Plan of Guangzhou City (201607010322), the LanDun information security technology open fund (LD20170210), and the Innovation Project of Graduate School of South China Normal University (2017LKXM081).

References

1. Qu LN, Hou XH, Huang XY, Liang Q, Ru Q, Wu B, Lam KH (2017) Self-assembled porous NiFe_2O_4 floral microspheres inlaid on ultrathin flake graphite as anode materials for Lithium batteries. *ChemElectroChem* 4:3148–3155. <https://doi.org/10.1002/celec.201700862>
2. Huang ZJ, Wang ZX, Jing Q, Guo H, Li X, Yang Z (2016) Investigation on the effect of Na doping on structure and Li-ion kinetics of layered $\text{LiNi}_{0.6}\text{Co}_{0.2}\text{Mn}_{0.2}\text{O}_2$ cathode material. *Electrochim Acta* 192:120–126. <https://doi.org/10.1016/j.electacta.2016.01.139>
3. Chen HD, Hou XH, Qu LN, Qin H, Ru Q, Huang Y, Hu S, Lam KH (2017) Electrochemical properties of core-shell nano-Si@carbon composites as superior anode materials for high-performance Li-ion batteries. *J Mater Sci Mater Electron* 28:250–258. <https://doi.org/10.1007/s10854-016-5518-x>
4. Xu JT, Ma JM, Fan QH, Guo S, Dou S (2017) Recent progress in the design of advanced cathode materials and battery models for high-performance Lithium-X (X = O_2 , S, Se, Te, I_2 , Br_2) batteries. *Adv Mater* 29:1–20. <https://doi.org/10.1002/adma.201606454>
5. Kolek M, Otteny F, Schmidt P, Mück-Lichtenfeld C, Einholz C, Becking J, Schleicher E, Winter M, Bieker P, Esser B (2017) Ultra-high cycling stability of poly(vinylphenothiazine) as a battery cathode material resulting from π - π interactions. *Energy Environ Sci* 10:2334–2341. <https://doi.org/10.1039/c7ee01473b>
6. Huang YL, Hou XH, Ma SM, Zou X, Wu Y, Hu S, Shao Z, Liu X (2015) Template GN-L-assisted synthesis of porous $\text{Li}_{1.2}\text{Mn}_{0.534}\text{Ni}_{0.133}\text{Co}_{0.133}\text{O}_2$: towards high performance cathodes for lithium ion batteries. *RSC Adv* 5:25258–25265. <https://doi.org/10.1039/c5ra00845j>
7. Yao J, Wang XL, Zhao XR et al (2016) Electrospun Li_2MnO_3 -modified $\text{Li}_{1.2}\text{Ni}_x\text{Co}_{0.1}\text{Mn}_{0.9-x}\text{O}_2$ nanofibers: synthesis and enhanced electrochemical performance for lithium-ion batteries. *Electron Mater Lett* 12:804–811. <https://doi.org/10.1007/s13391-016-6171-5>
8. Tan SY, Wang L, Bian L, Xu JB, Ren W, Hu PF, Chang AM (2015) Highly enhanced low temperature discharge capacity of $\text{LiNi}_{1/3}\text{Co}_{1/3}\text{Mn}_{1/3}\text{O}_2$ with lithium boron oxide glass modification. *J Power Sources* 277:139–146. <https://doi.org/10.1016/j.jpowsour.2014.11.149>
9. Kobayashi G, Irii Y, Matsumoto F, Ito A, Ohsawa Y, Yamamoto S, Cui Y, Son JY, Sato Y (2016) Improving cycling performance of Li-rich layered cathode materials through combination of Al_2O_3 -based surface modification and stepwise precycling. *J Power Sources* 303:250–256. <https://doi.org/10.1016/j.jpowsour.2015.11.014>

10. Liang LW, Du K, Peng ZD et al (2014) Co-precipitation synthesis of $\text{Ni}_{0.6}\text{Co}_{0.2}\text{Mn}_{0.2}(\text{OH})_2$ precursor and characterization of $\text{LiNi}_{0.6}\text{Co}_{0.2}\text{Mn}_{0.2}\text{O}_2$ cathode material for secondary lithium batteries. *Electrochim Acta* 130:82–89. <https://doi.org/10.1016/j.electacta.2014.02.100>
11. Xia H, Lu L, Meng YS, Ceder G (2007) Phase transitions and high-voltage electrochemical behavior of LiCoO_2 thin films grown by pulsed laser deposition. *J Electrochem Soc* 154:A337–A342. <https://doi.org/10.1149/1.2509021>
12. Guo B, Zhao JH, Fan XM, Zhang W, Li S, Yang Z, Chen Z, Zhang W (2017) Aluminum and fluorine co-doping for promotion of stability and safety of lithium-rich layered cathode material. *Electrochim Acta* 236:171–179. <https://doi.org/10.1016/j.electacta.2017.03.133>
13. Liu H, Cao Q, Fu LJ et al (2006) Doping effects of zinc on LiFePO_4 cathode material for lithium ion batteries. *Electrochem. Commun* 8:1553–1557. <https://doi.org/10.1016/j.elecom.2006.07.014>
14. Wu CY, Huang W, Liu LF, Wang H, Zeng Y, Xie J, Jin C, Zhang Z (2016) Facile synthesis of hierarchical $\beta\text{-LiFePO}_4$ and its phase transformation to electrochemically active $\alpha\text{-LiFePO}_4$ for Li-ion batteries. *CrystEng Comm* 18:7707–7714. <https://doi.org/10.1039/c6ce01294a>
15. Wang FX, Xiao SY, Zhu YS, Chang Z, Hu CL, Wu YP, Holze R (2014) Spinel LiMn_2O_4 nanohybrid as high capacitance positive electrode material for supercapacitors. *J Power Sources* 246:19–23. <https://doi.org/10.1016/j.jpowsour.2013.07.046>
16. Wang FX, Xiao SY, Gao XW, Zhu YS, Zhang HP, Wu YP, Holze R (2013) Nanoporous LiMn_2O_4 spinel prepared at low temperature as cathode material for aqueous supercapacitors. *J Power Sources* 242:560–565. <https://doi.org/10.1016/j.jpowsour.2013.05.115>
17. Wang SF, Sha YJ, Zhu YL, Xu X, Shao Z (2015) Modified template synthesis and electrochemical performance of a Co_3O_4 /mesoporous cathode for lithium-oxygen batteries. *J Mater Chem A* 3:16132–16141. <https://doi.org/10.1039/C5TA03091A>
18. Wang SF, Suo Y, Su C, Chen Y, Zhu Y, Shao Z (2016) Graphene decorated with multiple nanosized active species as dual function electrocatalysts for lithium-oxygen batteries. *Electrochim Acta* 188:718–726. <https://doi.org/10.1016/j.electacta.2015.12.046>
19. Wang FX, Xiao SY, Shi Y, Liu LL, Zhu YS, Wu YP, Wang JZ, Holze R (2013) Spinel $\text{LiNi}_x\text{Mn}_{2-x}\text{O}_4$ as cathode material for aqueous rechargeable lithium batteries. *Electrochim Acta* 93:301–306. <https://doi.org/10.1016/j.electacta.2013.01.106>
20. Tang ZH, Zheng HH, Qian FP, Ma Y, Zhao C, Song L, Chen Y, Xiong X, Zhu X, Mi C (2018) Improvement of cycling and thermal stability of $\text{LiNi}_{0.8}\text{Mn}_{0.1}\text{Co}_{0.1}\text{O}_2$ cathode material by secondly treating process. *Ionics* 24:61–71. <https://doi.org/10.1007/s11581-017-2179-6>
21. Kasnatscheew J, Evertz M, Streipert B, Wagner R, Klöpsch R, Vortmann B, Hahn H, Nowak S, Amereller M, Gentschev AC, Lamp P, Winter M (2016) The truth about the 1st cycle coulombic efficiency of $\text{LiNi}_{1/3}\text{Co}_{1/3}\text{Mn}_{1/3}\text{O}_2$ (NCM) cathodes. *Phys Chem Chem Phys* 18:3956–3965. <https://doi.org/10.1039/c5cp07718d>
22. Liu W, Oh P, Liu X, Lee MJ, Cho W, Chae S, Kim Y, Cho J (2015) Nickel-rich layered lithium transition-metal oxide for high-energy lithium-ion batteries. *Angew Chem Int Ed* 54:4440–4457. <https://doi.org/10.1002/anie.201409262>
23. Yao L, Feng Y, Xi GX (2015) A new method for the synthesis of $\text{LiNi}_{1/3}\text{Co}_{1/3}\text{Mn}_{1/3}\text{O}_2$ from waste lithium ion batteries. *RSC Adv* 5:44107–44114. <https://doi.org/10.1039/C4RA16390G>
24. Lu C, Wu H, Zhang Y, Liu H, Chen B, Wu N, Wang S (2014) Cerium fluoride coated layered oxide $\text{Li}_{1.2}\text{Mn}_{0.54}\text{Ni}_{0.13}\text{Co}_{0.13}\text{O}_2$ as cathode materials with improved electrochemical performance for lithium ion batteries. *J Power Sources* 267:682–691. <https://doi.org/10.1016/j.jpowsour.2014.05.122>
25. Hu CL, Yi HH, Wang FX, Xiao SY, Wu YP, Wang D, He DL (2014) Boron doping at P-site to improve electrochemical performance of LiMnPO_4 as cathode for lithium ion battery. *J Power Sources* 255:355–359. <https://doi.org/10.1016/j.jpowsour.2013.12.040>
26. Xie HB, Du K, Hu GR et al (2016) The role of sodium in $\text{LiNi}_{0.8}\text{Co}_{0.15}\text{Al}_{0.05}\text{O}_2$ cathode material and its electrochemical behaviors. *J Phys Chem C* 120:3235–3241. <https://doi.org/10.1021/acs.jpcc.5b12407>
27. Jiang YX, Zhou F, Wang CL, Kong J, Xu L (2017) Influence of co-precipitation temperature on microstructure and electrochemical properties of $\text{Li}[\text{Li}_{0.2}\text{Mn}_{0.54}\text{Ni}_{0.13}\text{Co}_{0.13}]\text{O}_2$ cathode materials for lithium ion batteries. *Ionics* 23:585–596. <https://doi.org/10.1007/s11581-016-1863-2>
28. Zhao RR, Yang ZL, Liang JX, Lu D, Liang C, Guan X, Gao A, Chen H (2016) Understanding the role of Na-doping on Ni-rich layered oxide $\text{LiNi}_{0.5}\text{Co}_{0.2}\text{Mn}_{0.3}\text{O}_2$. *J Alloy Compd* 689:318–325. <https://doi.org/10.1016/j.jallcom.2016.07.230>
29. Chen Z, Wang J, Chao DL, Baikie T, Bai L, Chen S, Zhao Y, Sum TC, Lin J, Shen Z (2016) Hierarchical porous $\text{LiNi}_{1/3}\text{Co}_{1/3}\text{Mn}_{1/3}\text{O}_2$ Nano-/micro spherical cathode material: minimized cation mixing and improved Li^+ mobility for enhanced electrochemical performance. *Sci Rep* 6:25771. <https://doi.org/10.1038/srep25771>
30. Wang YX, Shang KH, He W, Ai XP, Cao YL, Yang HX (2015) Magnesium-doped $\text{Li}-1.2[\text{Co}_{0.13}\text{Ni}_{0.13}\text{Mn}_{0.54}]\text{O}-2$ for Lithium-ion battery cathode with enhanced cycling stability and rate capability. *ACS Appl Mater Interfaces* 7:13014–13021. <https://doi.org/10.1021/acsami.5b03125>
31. Jiang L, Fu CP, Li KQ, Zhou H, Huang Y, Kuang Y (2017) K-doped $\text{Li}_3\text{V}_2(\text{PO}_4)_3$: a novel cathode material for high performance lithium-ion batteries. *Mater Lett* 198:73–75. <https://doi.org/10.1016/j.matlet.2017.04.014>
32. Chen L, Gu QW, Zhou XF et al (2013) New-concept batteries based on aqueous Li^+/Na^+ mixed-ion electrolytes. *Sci. Rep* 3:1946. <https://doi.org/10.1038/srep01946>
33. Wang JX, Wang ZX, Li XH, Guo H, Wu X, Zhang X, Xiao W (2013) $x\text{Li}_3\text{V}_2(\text{PO}_4)_3\text{-LiVPO}_4\text{F/C}$ composite cathode materials for lithium ion batteries. *Electrochim Acta* 87:224–229. <https://doi.org/10.1016/j.electacta.2012.09.014>
34. Shi SJ, Tu JP, Mai YJ, Zhang YQ, Gu CD, Wang XL (2012) Effect of carbon coating on electrochemical performance of $\text{Li}_{1.048}\text{Mn}_{0.381}\text{Ni}_{0.286}\text{Co}_{0.286}\text{O}_2$ cathode material for lithium-ion batteries. *Electrochim Acta* 63:112–117. <https://doi.org/10.1016/j.electacta.2011.12.082>
35. Zheng JM, Wu XBYY (2011) A comparison of preparation method on the electrochemical performance of cathode material $\text{Li}[\text{Li}_{0.2}\text{Mn}_{0.54}\text{Ni}_{0.13}\text{Co}_{0.13}]\text{O}_2$ for lithium ion battery. *Electrochim Acta* 56:3071–3078. <https://doi.org/10.1016/j.electacta.2010.12.049>
36. Kim H-J, Jin B-S, Doh C-H, Bae D-S, Kim HS (2013) Improved electrochemical performance of doped- $\text{LiNi}_{0.5}\text{Mn}_{1.5}\text{O}_4$ cathode material for lithium-ion batteries. *Electron Mater Lett* 9:851–854. <https://doi.org/10.1007/s13391-013-6028-0>